ELSEVIER

Journal of Fluids and Structures 18 (2003) 635–650

JOURNAL OF FLUIDS AND STRUCTURES

www.elsevier.nl/locate/jnlabr/yjfls

Turbulence-induced fluid dynamic forces acting on cross-shaped tube bundle in cross-flow

T. Nishihara[a,*], F. Inada[b], A. Yasuo[b], R. Morita[b], A. Sakashita[c], J. Mizutani[c]

[a] *Fluid Science Department, Central Research Institute of Electric Power Industry (CRIEPI), 1646 Abiko, Abiko-shi Chiba 270-1194, Japan*

[b] *Central Research Institute of Electric Power Industry (CRIEPI), 2-11-1, Iwado-Kita, Komae-shi, Tokyo 201-8511, Japan*

[c] *Tokyo Electric Power Company, 1-1-3 Uchisaiwai-cho, Chiyoda-ku, Tokyo 100-0011, Japan*

Received 22 October 2002; accepted 9 August 2003

Abstract

A cross-shaped tube bundle with small ratio of the gap width to tube diameter may be designed for the lower plenum structure in a next-generation BWR, though the characteristics of flow-induced vibration of this type of tube bundle remain virtually unknown. In this study, fluid dynamic forces acting on a cross-shaped tube bundle in a normal arrangement with small ratio of the gap width to tube diameter subjected to cross-flow were measured by water tunnel tests with two types of scale model. One was a small-scale model to measure local fluid dynamic forces and their correlation length in the lift and drag directions. The other was a large-scale model to investigate the effect of the Reynolds number on fluid dynamic forces in the lift, drag and torsional directions. Free oscillation tests with another small-scale model were also conducted to measure vibration amplitude by random excitation force. The following results were obtained. The measured fluid dynamic drag, lift and torque acting on the cross-shaped tube bundle in cross-flow were successfully compiled into the correlation equations, which include the nondimensional power spectral density (NPSD) of the local fluid dynamic force and the spanwise correlation length. The Reynolds effects on the NPSD can be considered negligible at least in the range of Reynolds number $<10^6$. No remarkable spectral peaks of vortex shedding appeared in the NPSD, and the ratios of the correlation lengths to the tube diameter for the cross-shaped tube bundle were much shorter than that of the random excitation force acting on circular tube bundles. It is considered that this was because the ratio of gap width to tube diameter was small for the tested arrangement.
© 2003 Elsevier Ltd. All rights reserved.

1. Introduction

When designing a plant structure subjected to flow, it is desirable to evaluate flow-induced vibrations in order to confirm the long-term integrity of the structure. With tube bundles, which are familiar structures in heat exchangers, the stress amplitude caused by turbulence-induced vibrations needs to be estimated, and both fluid-elastic vibrations and vortex-induced vibrations have to be avoided. Many studies have been conducted on flow-induced vibrations on circular tube bundles, as reviewed in depth by Chen (1987), Weaver and Fitzpatrick (1988), Blevins (1990), Au-Yang (2001), and so on. A guideline for evaluating the flow-induced vibration of circular tube bundles is given in the ASME Boiler and Pressure Vessel Code (1998).

Regarding turbulence-induced vibrations of circular tube bundles, the characteristics of turbulence excitation forces have been investigated experimentally by many researchers such as Blevins et al. (1981), Pettigrew and Gorman (1981),

*Corresponding author. Tel.: +81-4-71821181; fax: +81-4-71847142.
E-mail address: shake@criepi.denken.or.jp (T. Nishihara).

0889-9746/$ - see front matter © 2003 Elsevier Ltd. All rights reserved.
doi:10.1016/j.jfluidstructs.2003.08.014

Nomenclature

D	tip-to-tip diameter of cross-shaped tube
f	frequency
f_n	natural frequency
f^*	nondimensional frequency
I_p	inertia moment of cross-shaped tube in torsional direction
l	length of structure
Re	Reynolds number
S	one-sided power spectral density or cross-spectral density of local fluid dynamic force
S'	one-sided power spectral density of fluid dynamic force acting on tubes with finite spanwise length
T	transverse pitch
U_g	gap flow velocity
U_∞	incident flow velocity
W_g	reference gap width
x	axis in spanwise direction
Φ	one-sided nondimensional power spectral density of random excitation force or torque
ζ_n	structural damping ratio
η	λ/l
θ	angular displacement
λ	correlation length of fluid dynamic force
ν	kinematic viscosity
ρ	density of fluid
ω_n	natural angular frequency

Chen and Jendrzejczyk (1987), Axisa et al. (1990), and Inada et al. (1993, 2001). Au-Yang (1999) reviewed the theoretical development of the acceptance integral method to estimate the random vibration of structures subjected to turbulent flow.

A cross-shaped tube has been proposed for the control-rod guide tube of the next-generation BWR instead of a circular tube, in which case the lower-plenum structure will be a cross-shaped tube bundle (Yamashita et al., 2001), even though cross-shaped tubes have rarely been used in practical engineering structures. There have also been few studies on flow-induced vibrations of a cross-shaped tube bundle, and their characteristics remain largely unknown. Consequently, it is necessary to investigate their characteristics and to develop methods for predicting them. Inada et al. (2002, 2003) measured the vibration response of a cross-shaped tube bundle to clarify the characteristics of self-excited vibration and proposed a guideline to avoid it.

In this study, water tunnel tests with two types of scale model were conducted to investigate the characteristics of the fluid excitation forces acting on a cross-shaped tube bundle in a normal arrangement subjected to a cross-flow. Local fluid dynamic forces and their correlation length in the lift and drag directions were measured with a small-scale model of a practical plant now being planned. The effect of Reynolds number on fluid dynamic forces was investigated by a large-scale model. From the experimental results, dimensionless correlation equations that include the nondimensional power spectral density (NPSD) and spanwise correlation length for the local fluid dynamic forces were derived. Free oscillation tests with another small-scale model were also conducted to measure vibration amplitude by random excitation force to examine the validity of the proposed correlation equations.

2. Experimental arrangement

2.1. Experimental apparatus of small-scale model

Figs. 1 and 2 show the experimental apparatus of the small-scale model tests for measuring local fluid dynamic forces and their spanwise correlation length.

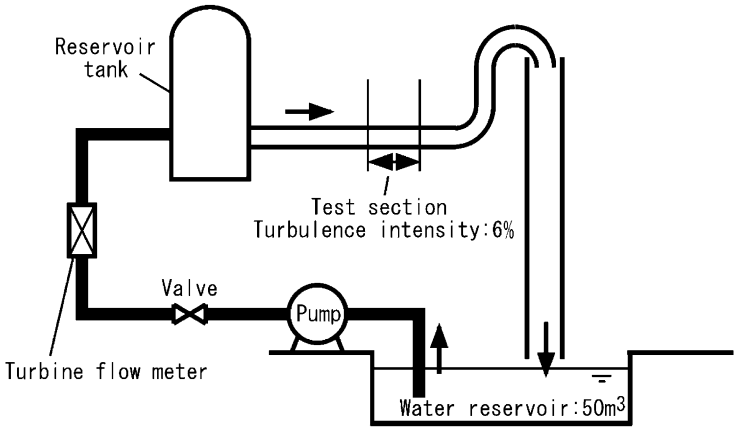

Fig. 1. Test loop for the small-scale model tests.

A schematic diagram of the test loop for the small-scale test is shown in Fig. 1. The loop is a water circuit, with a test-section which measures 300 mm in width and 280 mm in depth in the transverse direction against the flow and 400 mm long in the streamwise direction. The flow is provided by a pump and is passed through a turbine flow meter, a surge tank and a flow rectifier, and then enters the test-section. The flow rate is measured by a turbine flow meter. The turbulence intensity of the incident flow into the test-section is about 6% of the steady flow velocity, which was preliminarily measured with a hot film at the entrance of the test-section.

Figs. 2(a) and (b) show the small-scale model of the cross-shaped tube bundle arranged in the test-section. The model consists of cross-shaped tubes, which simulate the outer shape of the cross-section of the tube designed for the planned practical plant. The reference diameter D of the cross-shaped tubes shown in Fig. 2(a) is about 90 mm and the spanwise length is 280 mm. A normal arrangement of five rows with four columns per row is used for this investigation. The transverse pitch is about 75 mm and the minimum gap width shown in Fig. 2(a) is about 8 mm. The tubes are subjected to a cross-flow entering the test-section. The four tubes (colored white in Fig. 2(a)) are for the fluid dynamic force measurement, while the other tubes are dummies.

The sensing mechanism of the local fluid dynamic forces is shown in Fig. 2(c). The fluid dynamic forces acting on cross-shaped sensing parts of 12 mm-width installed in the tubes were measured in the small-scale model tests. The sensing part is elastically mounted on the stainless steel shaft through a spring plate to form a spring-mass system. Waterproof strain gauges are stuck to both surfaces of the spring plate. In a preliminary calibration test of the sensing mechanism, a weight was hung on the sensing part, and the magnitude of the force acting on the sensing part was correlated to the output of the strain gauges. If the natural frequency of the sensing system is much higher than the objective frequency of the fluid force, the sensing part nearly corresponds to the fluid dynamic force statically, and the strain gauge outputs can be reduced to the amplitudes of the fluid dynamic forces according to the static calibration tests. Generally, the error is within the range of 20% on condition that the minimum natural frequency of the sensing system is three times higher than that of the input dynamic force. The minimum natural frequency of the sensing system in water is about 70 Hz according to hammering tests, so measured fluid dynamic forces under 25 Hz were adopted in the tests. Four sensing parts spaced 34 mm apart were installed in each tube, so the local fluid dynamic forces were measured at 16 points simultaneously.

It should be noted that the sensing mechanism responds to a force in one direction, and cannot simultaneously measure the drag and lift. In the small-scale tests, the dynamic lift was measured first, then the tubes with the sensing mechanism were rotated 90° around the tube axis and the dynamic drag was measured.

2.2. Experimental apparatus of large-scale model

Figs. 3 and 4 schematically show the experimental apparatus of the large-scale model used for the tests conducted at high Reynolds number.

The vertical water tunnel of the gravitational draining type shown in Fig. 3 was used for the tests. It consists of an underground reservoir of 1700 m^3, an upper reservoir of 40 m^3, a vertical water tunnel section and a draining valve. Before the tunnel is operated, water is pumped up from the underground reservoir to the upper reservoir with the draining valve closed. Once the upper reservoir has been filled with water, the valve is opened and the water flows into

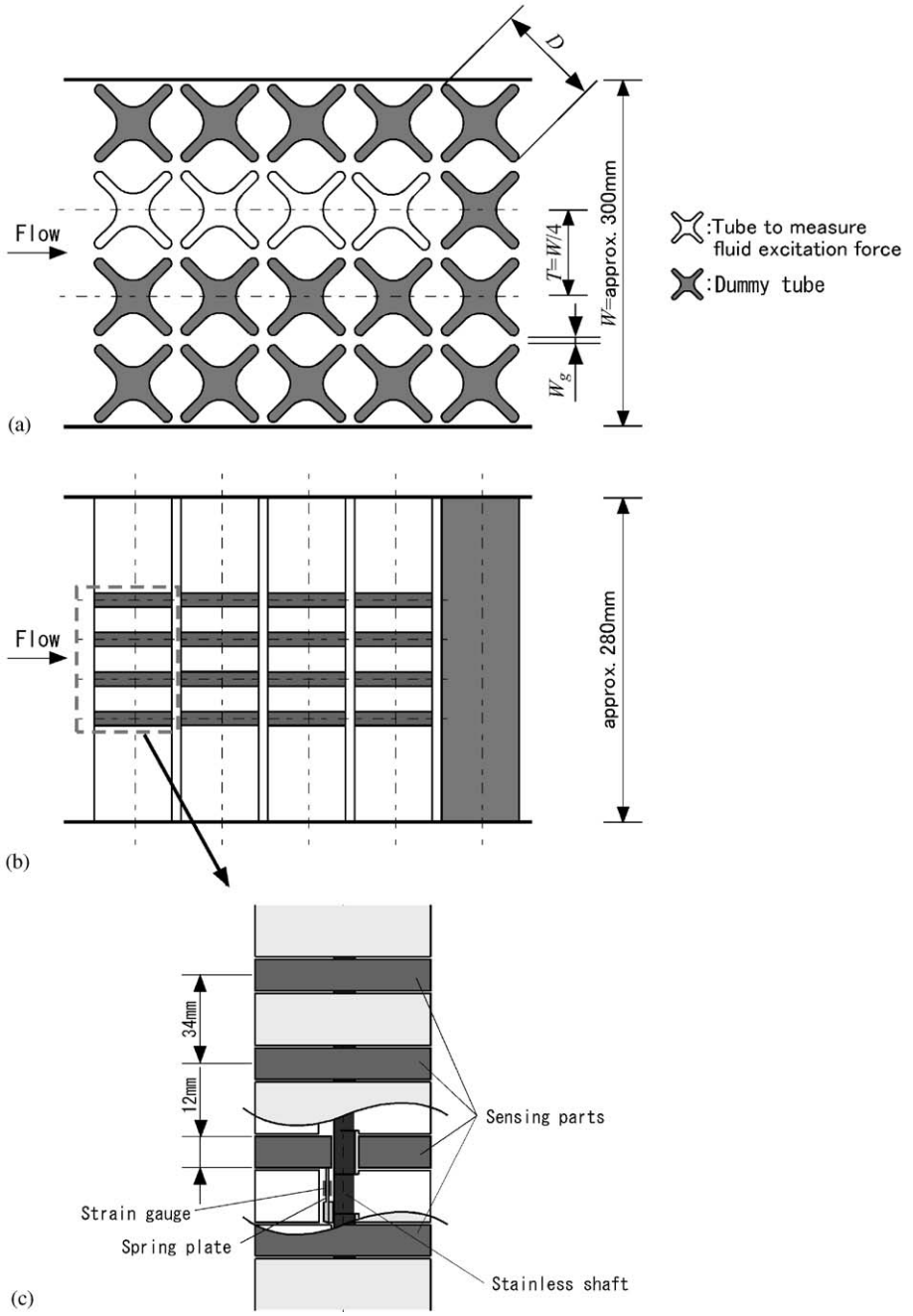

Fig. 2. Test tubes of small-scale model arranged in test-section: (a) side view; (b) top view; and (c) sensing mechanism to measure local fluid dynamic force.

the test-section through the contraction driven by gravitational force and drains into the underground reservoir through the valve. With this kind of water tunnel, experiments with a high flow rate can be conducted without requiring a high-power pump. The test-section is rectangular with a width of 1000 mm and depth of 500 mm. The incident flow velocity is measured by an electromagnetic current meter during the fluid force measurement. The turbulence intensity of the incident flow is about 1.5% of the steady flow velocity according to preliminary measurements by Laser Doppler velocimetry.

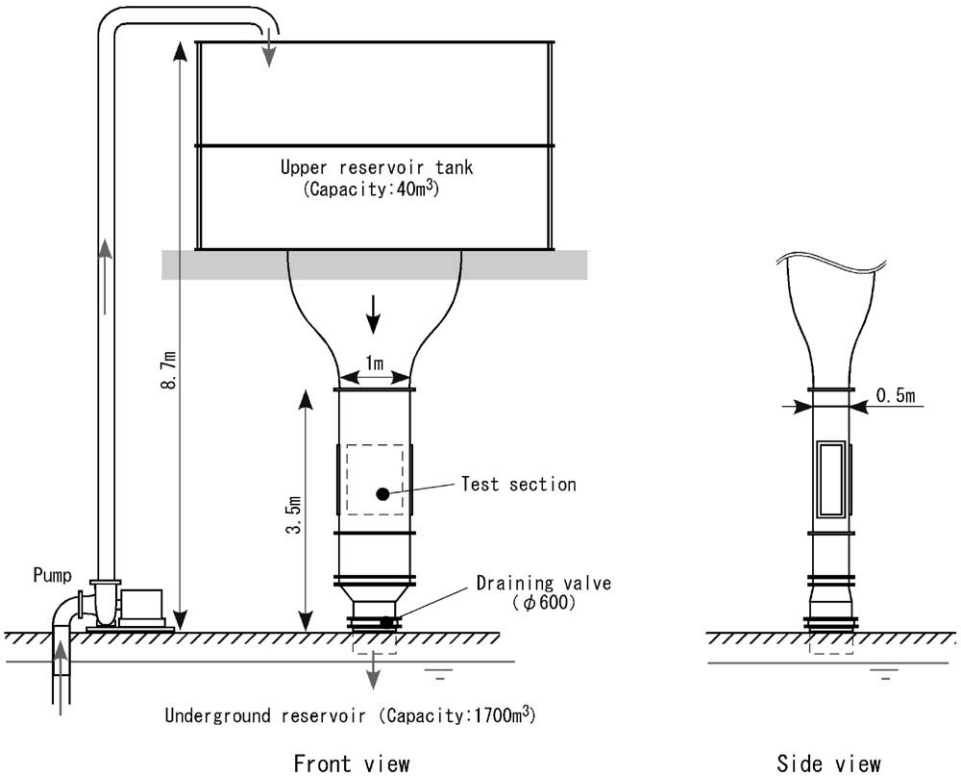

Fig. 3. Test loop for large-scale model tests.

A schematic of the large-scale model of the cross-shaped tube bundle is shown in Fig. 4. A normal arrangement of four rows with three tubes per row is used for the tests. The reference length D of the model tube is approximately 200 mm and the reference gap width is approximately 19 mm. The transverse pitch T is approximately 170 mm. The tubes are subjected to a cross-flow entering the test-section.

The fluid dynamic forces acting on the center tubes in the second and third rows were measured in the large-scale model tests. Both ends of the two tubes are supported elastically through the supporting parts shown in Fig. 4(b). The supporting part has a cylindrical section with an outer diameter of 34 mm and inner diameter of 30 mm. Strain gauges are fitted on the inner surface of the cylindrical section. Their outputs were correlated to the magnitude of the static forces in the lift, drag and torsional directions acting on the tube by preliminary calibration tests of hanging a weight. The fluid dynamic forces acting on the whole span of the tube were estimated by the strain gauge outputs. The measured fluid dynamic forces under 40 Hz in the lift and drag directions, and those under 50 Hz in the torsional direction are adopted because the natural frequencies of the two tubes in water are 129 and 150 Hz, respectively.

2.3. Experimental conditions

All experiments were conducted under conditions of normal pressure and normal temperature. Summaries of the model specifications and experimental conditions are shown in Table 1. The Reynolds number is defined by the following equation in terms of the gap flow velocity U_g:

$$\mathrm{Re} = U_g D/\nu, \tag{1}$$

where the reference length D is the tip-to-tip diameter of the cross-shaped tubes. The gap flow velocity U_g is given by

$$U_g = U_\infty \frac{T}{W_g}, \tag{2}$$

where U_∞ is the incident flow velocity, T is the transverse pitch, and W_g is the minimum gap width shown in Figs. 2(a) and 4(a).

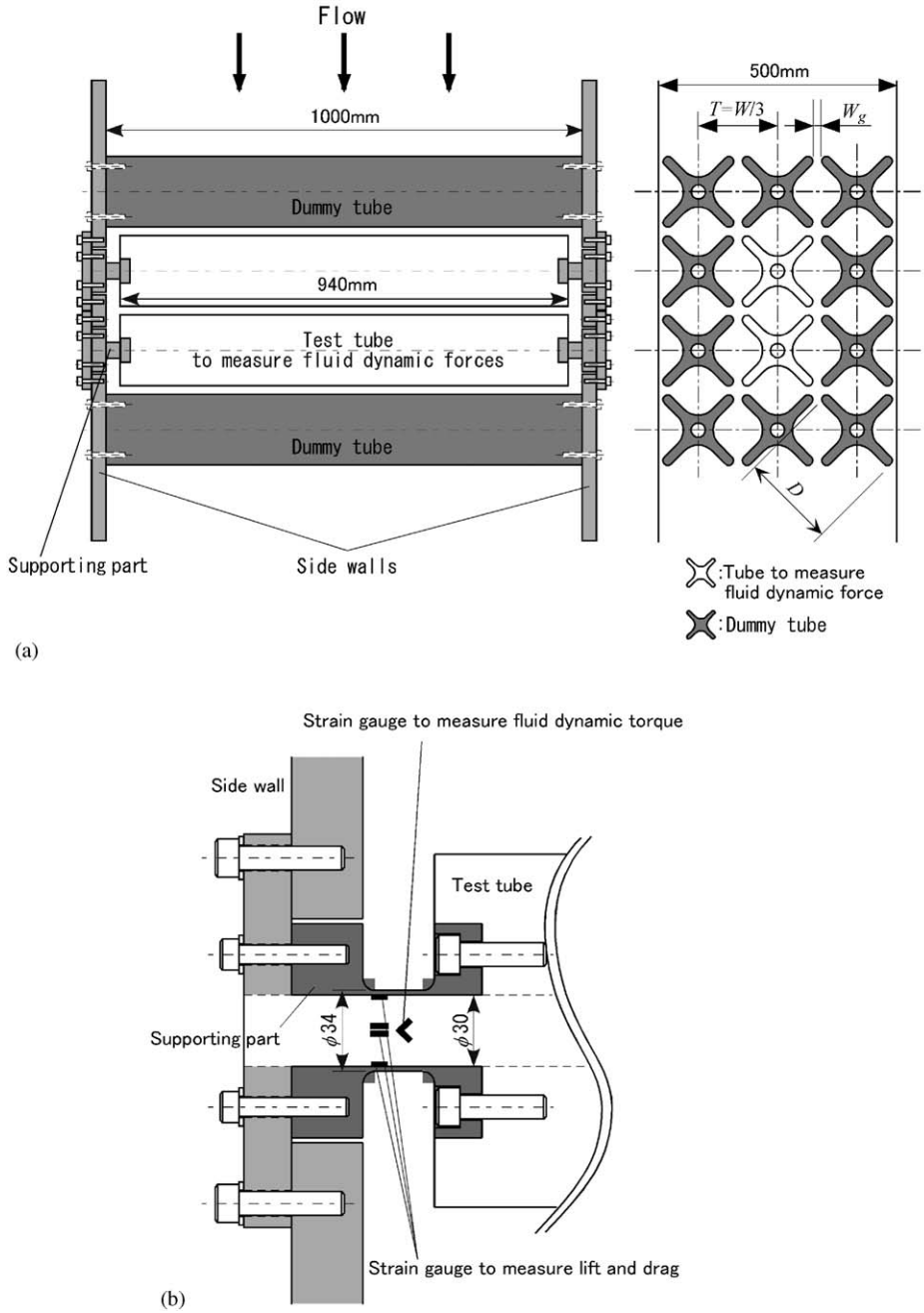

Fig. 4. Test tubes of large-scale model arranged in test-section: (a) Layout of the tubes in the test-section and (b) sensing mechanism to measure fluid forces.

Table 1
Experimental conditions

	Small-scale model	Large-scale model
Diagonal diameter	approx. 90 mm	approx. 200 mm
Gap flow velocity	0.45–3.6 m/s	3.4–6.0 m/s
Reynolds Number	4×10^4–3.2×10^5	6.8×10^5–1.2×10^6

3. Experimental results of small-scale model tests

3.1. Characteristics of PSD and CSD of fluid dynamic force

Fig. 5 shows typical power spectral densities (PSD) of the dynamic lift force acting on a sensing ring of each tube in the first through fourth row. Each PSD gradually decreases as frequency increases, and no remarkable spectral peaks appear. In the case of circular tube bundles, spectral peaks of vortex shedding are often observed, as reviewed by Weaver and Fitzpatrick (1988) and Blevins (1990), and these are a potential cause of acoustic resonance as well as vortex-induced vibration. However, these distinct frequency components of vortex shedding degenerate into a broad-band spectrum in closely spaced tube arrays with a pitch-to-diameter ratio of less than 1.5 (Blevins, 1990). Accordingly, the result shown in Fig. 5 with no remarkable spectral peaks is considered reasonable, because the gap width is approximately one-tenth of the reference diameter in the tested arrangement of the cross-shaped tubes. The PSD of the dynamic lift force acting on the tube in the first row is smaller than those acting on the tubes downstream. The PSDs in the second thru fourth row almost coincide, which suggests that they are almost saturated downstream of the second row.

Fig. 6 shows the typical PSD of dynamic lift force acting on the sensing ring and the amplitude of the cross-spectral density (CSD) between the forces acting on the adjoining sensing rings installed on the same tube. The PSD and the amplitude of the CSD shown in Fig. 6(a) are parallel to each other. Fig. 6(b) shows the phases of the CSD and they are scattered around zero. According to Axisa et al. (1990) and Au-Yang (1999), the coherence function $\Gamma(x_1, x_2, f)$, which characterizes the turbulence-induced excitation force acting on a cylindrical structure, is generally defined as follows:

$$\Gamma(x_1, x_2, f) = \frac{S(x_1, x_2, f)}{S(x_1, x_1, f)}, \tag{3}$$

where $S(x_1, x_1, f)$ and $S(x_1, x_2, f)$ are the PSD and CSD of the local fluid dynamic force, which acts on the infinitesimally narrow width of the cylindrical structure, respectively, and x_1 and x_2 are two different points on the structure. Many researchers assume that the coherence function $\Gamma(x_1, x_2, f)$ can be expressed as follows:

$$\Gamma(x_1, x_2, f) = \exp\left(-\frac{|x_1 - x_2|}{\lambda}\right) \cdot \exp\left(-\frac{\mathrm{i}2\pi f(x_1 - x_2)}{U_c}\right), \tag{4}$$

where λ is the spanwise correlation length of the fluid dynamic force and U_c is the convective velocity. For straight tubes subjected to a uniform cross flow, the fluctuations are not advected along the tube and the coherence function reduces to a real function as follows:

$$\Gamma(x_1, x_2, f) = \exp\left(-\frac{|x_1 - x_2|}{\lambda}\right). \tag{5}$$

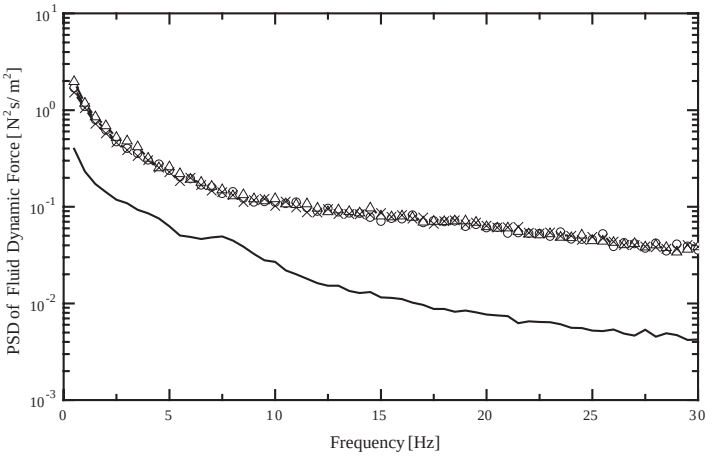

Fig. 5. PSD of fluid dynamic force acting on cross-shaped tubes in 1st to 4th row: ——, 1st row; —○—, 2nd row; —△—, 3rd row; —×—, 4th row.

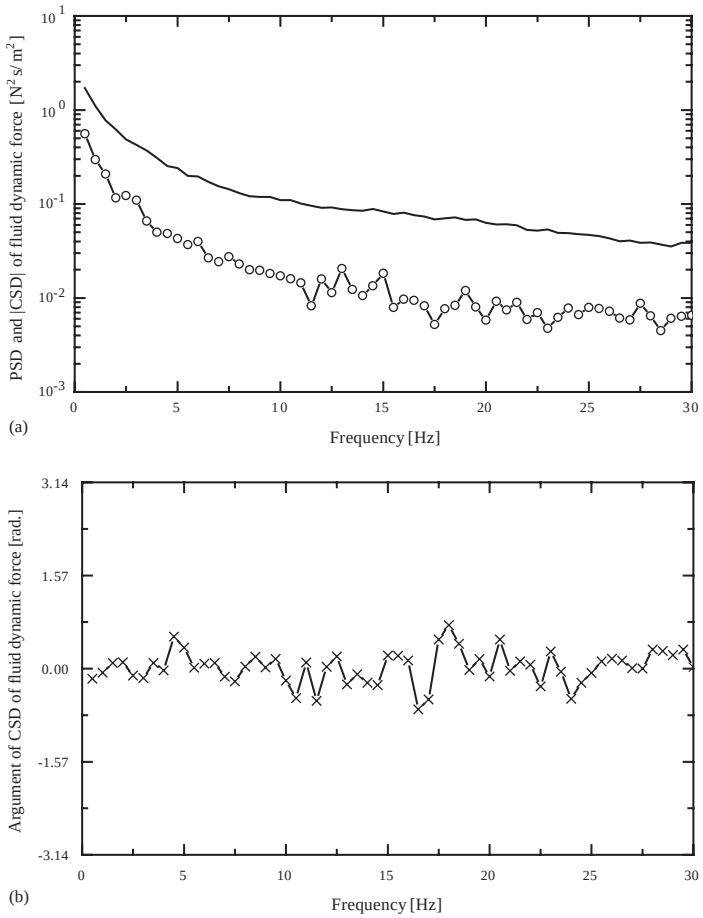

Fig. 6. PSD and CSD of local fluid dynamic force ($U_g = 1.03$ m/s): (a) (——) PSD, (—○—) amplitude of CSD and (b) argument of CSD.

For practical applications, it is reasonable to consider that the correlation length λ of the turbulence-induced excitation force is constant against varying frequency. The results shown in Fig. 6 confirm that these ideas are reasonable for the cross-shaped tube bundle as in the case of the circular tube bundle.

3.2. Estimation of PSD of local fluid dynamic force and correlation length

Since the spanwise width of the sensing ring is very narrow, the fluid dynamic force acting on the sensing rings is considered to be very close to the local fluid dynamic force, which acts on the infinitesimally narrow width of the tube. However, the sensing ring has a finite width of 12 mm, so the fluid dynamic force acting on the sensing rings does not coincide exactly with the local fluid dynamic force. In this section, the fluid dynamic forces measured by the sensing rings are converted to a set of the local fluid dynamic forces and their correlation length by the following procedures as described by Inada (1993, 2001).

Assuming Eq. (5), the following relations are obtained,

$$S'(x_1, x_1, f) = S(x_1, x_1, f) l^2 \psi_1(\eta), \tag{6}$$

$$S'(x_1, x_2, f) = S(x_1, x_2, f) l^2 \psi_2(\eta), \tag{7}$$

where $S'(x_1, x_1, f)$ and $S'(x_1, x_2, f)$ are the PSD and CSD of the fluid dynamic force acting on the sensing ring, respectively; l is the width of the sensing ring, and η, ψ_1 and ψ_2 are as follows:

$$\eta = \lambda / l, \tag{8}$$

$$\psi_1(\eta) = \int_0^1 \int_0^1 \exp\left(-\frac{|\xi' - \xi|}{\eta}\right) \mathrm{d}\xi \, \mathrm{d}\xi' = 2\eta^2 \left\{\frac{1}{\eta} - 1 + \exp\left(-\frac{1}{\eta}\right)\right\}, \tag{9}$$

$$\psi_2(\eta) = \int_0^1 \int_0^1 \exp\left(-\frac{\xi' - \xi}{\eta}\right) \mathrm{d}\xi \, \mathrm{d}\xi' = \eta^2 \left\{-2 + \exp\left(\frac{1}{\eta}\right) + \exp\left(-\frac{1}{\eta}\right)\right\}. \tag{10}$$

Using Eqs. (5)–(10), the PSD of local fluid dynamic force $S(x_1, x_1, f)$ and the correlation length λ can be obtained. First, λ can be expressed as follows:

$$\lambda = -\frac{|x_1 - x_2|}{\log\left((\psi_1(\eta)/\psi_2(\eta))\Gamma'\right)}, \tag{11}$$

$$\Gamma'(x_1, x_2, f) = \frac{S'(x_1, x_2, f)}{S'(x_1, x_1, f)}. \tag{12}$$

In Eq. (11), both ψ_1 and ψ_2 are a function of λ, so iterative calculation is needed to obtain λ.

When λ has been determined by the iteration with Eq. (11), η and ψ_1 can be given by Eqs. (8) and (9). Finally, the PSD of the local fluid dynamic force is obtained from Eq. (6) as follows:

$$S(x_1, x_1, f) = \frac{S'(x_1, x_1, f)}{(l^2 \psi_1(\eta))}. \tag{13}$$

For a typical example, Fig. 7(a) shows the coherence function $\Gamma'(x_1, x_2, f)$ of the measured dynamic lift force, which is necessary to estimate λ. The maximum value of the coherence $\Gamma'(x_1, x_2, f)$ is about 0.4 at most. In general, it is conservative to overestimate the coherence function with the exception of the lock-in range by vortex shedding. In view of the engineering utility of the correlation equation of fluid excitation forces, it is convenient to use a conservatively estimated constant value as the coherence function. Hence, the values of $\Gamma'(x_1, x_2, f)$ obtained by the experiments are arranged to the averaged value as the best estimated one, and the maximum value as the conservative one in this report. Fig. 7(a) indicates that the best estimated value and the conservative value of $\Gamma'(x_1, x_2, f)$ are 0.144 and 0.403, respectively. Therefore, the ratios of the correlation length to the reference diameter λ/D are calculated as 0.17 as the best-estimated value and 0.37 as the conservative one.

The PSD of the local dynamic fluid force can be obtained from Eq. (13), based on the correlation length calculated above. Fig. 7(b) shows the nondimensional PSD (NPSD) of the local dynamic lift force, which is defined by the following equation, as a function of nondimensional frequency:

$$\Phi(f^*) = \frac{S(f)}{\left(\frac{1}{2}\rho U_g^2 D\right)^2 (D/U_g)}. \tag{14}$$

The horizontal axis shows nondimensional frequency given by the following equation:

$$f^* = \frac{fD}{U_g}. \tag{15}$$

The NPSD of the local dynamic lift force gradually declines as f^* increases, and falls a little more rapidly in the region of $f^* > 1$. In all cases, no remarkable peaks corresponding to vortex shedding can be observed. Fig. 7(b) also reveals that the Reynolds number has little effect on the NPSD.

Fig. 8(a) shows the coherence function $\Gamma'(x_1, x_2, f)$ of the local dynamic drag force, and the correlation length and NPSD of the local dynamic drag force can be derived in the same way. Fig. 8(b) shows the NPSD as a function of nondimensional frequency. The NPSD of the local dynamic drag force has almost the same trend as that of the lift force against nondimensional frequency, and little effect of Reynolds number on the NPSD can be seen in those results.

The envelope of those NPSD curves is proposed as a correlation equation of the local dynamic force acting on the cross-shaped tube bundles in a normal arrangement. The correlation lengths and correlation equations proposed are summarized in Table 2. The obtained correlation lengths of the fluid dynamic forces acting on the cross-shaped tube bundle are about $0.17-0.18D$ as the best-estimated value, and are much shorter than that of the random excitation force acting on circular tube bundles. For instance, the correlation length λ of the random excitation force of the circular tube bundle is almost $1D$ according to measurements by Inada et al. (2001). This is considered to be because the ratio of the gap width to tube diameter is small in the tested arrangement of the cross-shaped tube bundles. In fact, λ is rather small and is about $0.45D$ for a circular tube bundle with a small pitch-to-diameter ratio of 1.26 (Inada et al., 1993). In general, the correlation length λ is scaled by a tube diameter D; however, if the correlation length λ is scaled by the gap width W_g, λ/W_g is $1.8 \sim 1.9$ for the tested cross-shaped tube bundle whereas λ/W_g is 1.7–1.8 for a circular tube

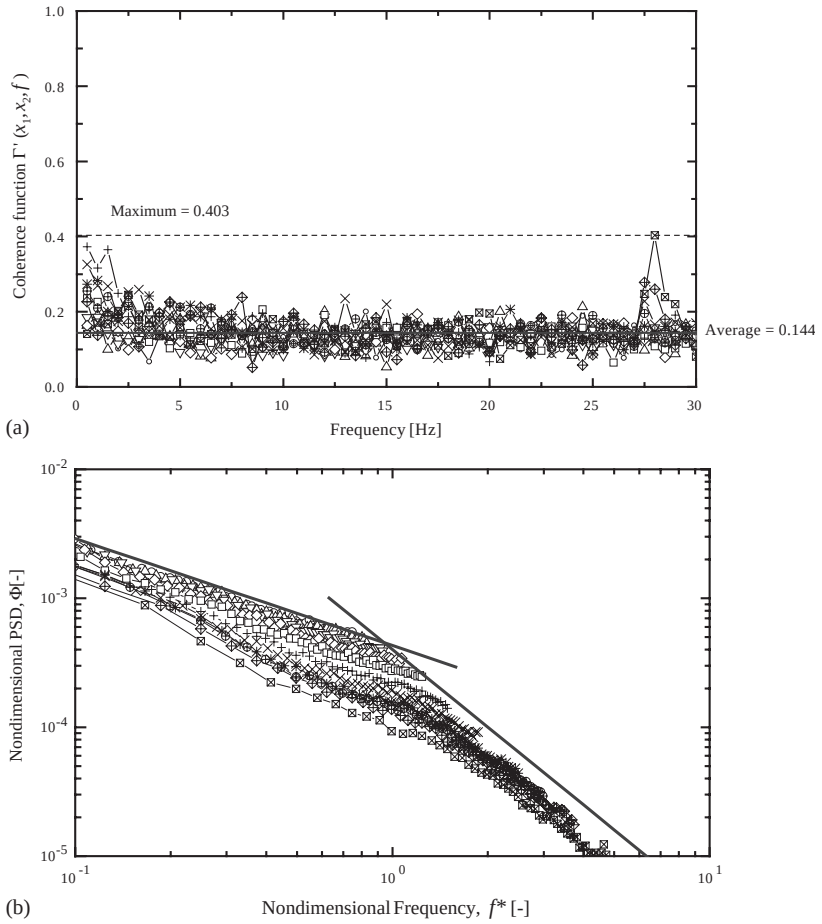

Fig. 7. Spanwise coherence function and nondimensional PSD of fluid dynamic force in the lift direction in case of normal arrangement: (a) spanwise coherence function and (b) Nondimensional PSD of local fluid dynamic force [Reynolds number: —○—, 3.2×10^5; —△—, 2.9×10^5; —▽—, 2.5×10^5; —◇—, 2.2×10^5; —□—, 1.9×10^5; —+—, 1.6×10^5; —×—, 1.2×10^5; –✳–, 9×10^4;—⊕—, 8×10^4; –⊕–, 6×10^4; —⊠—, 4×10^4. ——, envelope curve of NPSD.]

bundle with a pitch-to-diameter ratio of 1.26. They agree well with each other. The correlation length might be proportional to the gap width rather than the tube diameter when the ratio of the gap width to tube diameter is very small.

4. Experimental results of large-scale model tests

To investigate the Reynolds effect on the fluid dynamic forces acting on a cross-shaped tube bundles, large-scale model tests were conducted under high Reynolds number conditions. The experimental results are described below.

4.1. PSD of dynamic lift and drag force

Since the correlation length could not be measured by the large-scale model tests, the NPSD of the local fluid dynamic force in the large-scale model tests was calculated with the correlation length of the best estimation in the small-scale model tests by the following procedure.

The flexural rigidity of the tested cross-shaped tube of the large-scale model is large enough for the tube to be regarded as a rigid beam, compared with that of the cylindrical sensing parts supporting both ends of the tube. In this case, the joint acceptance of the fluid dynamic force acting on the test tube is expressed as Eq. (9), and the NPSD can be

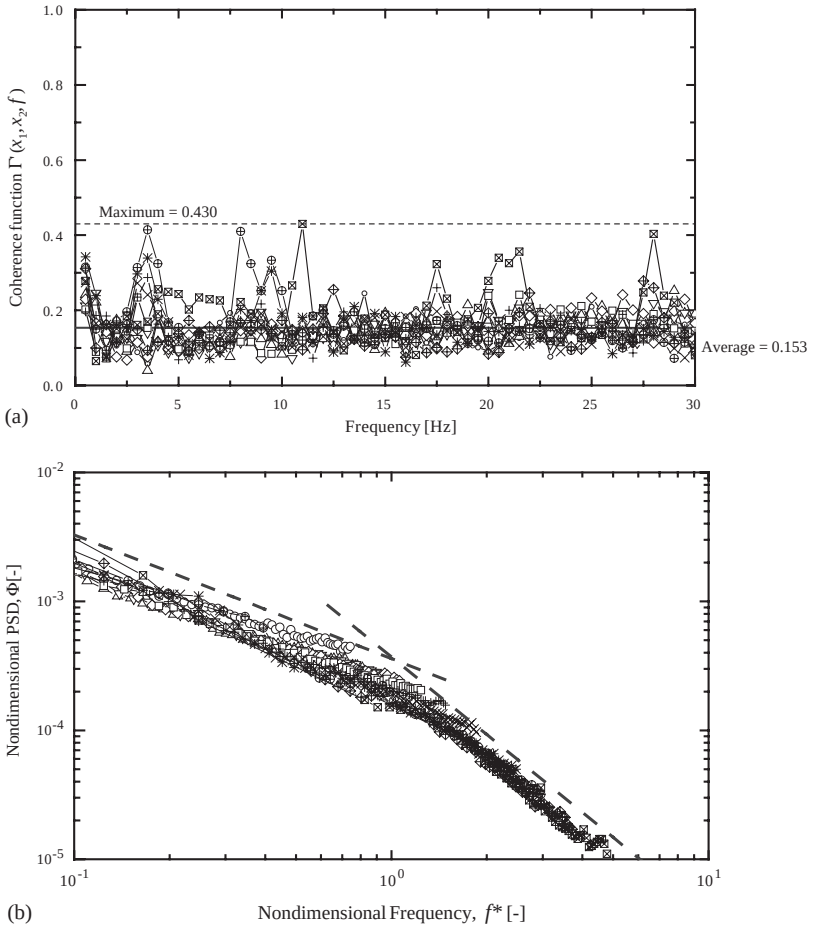

Fig. 8. Spanwise coherence function and nondimensional PSD of fluid dynamic force in the drag direction in case of normal arrangement: (a) spanwise coherence function and (b) nondimensional PSD of local fluid dynamic force [Reynolds number: —○—, 3.2×10^5; —△—, 2.9×10^5; —▽—, 2.5×10^5; —◇—, 2.2×10^5; —□—, 1.9×10^5; —+—, 1.6×10^5; —×—, 1.2×10^5; —✳—, 9×10^4; —⊕—, 8×10^4; —⊕—, 6×10^4; —⊠—, 4×10^4. ——, envelope curve of NPSD.]

Table 2
Nondimensional PSD and correlation length of local dynamic fluid force in lift and drag directions acting on cross-shaped tube

	a_1	a_2	Condition	λ/D
Lift	4.3×10^{-4}	−0.83	$f^*<0.9$	0.17/0.37[a]
	4.0×10^{-4}	−2.0	$f^*>0.9$	
Drag	3.6×10^{-4}	−0.96	$f^*<1.0$	0.18/0.39
	3.7×10^{-4}	−2.0	$f^*>1.0$	

Correlation equation: $\Phi(f^*)=a_1 f^{*a_2}$

[a] First entry—best fit; second entry—conservative.

calculated by the following equation, assuming that the ratio of the correlation length to tube diameter in the large-scale model tests is almost the same as for the small-scale model:

$$\Phi(f^*)=\frac{S'(f)}{l^2\psi_1(\eta)\left(\frac{1}{2}\rho U_g^2 D\right)^2(D/U_g)}, \tag{16}$$

where $S'(f)$ is the PSD of the fluid dynamic force measured in the large-scale model tests, $l = 0.94$ m, and η is as follows:

$$\eta = \frac{\lambda}{D}\frac{D}{l}. \tag{17}$$

Using $\lambda/D = 0.18$ of the dynamic drag force and $\lambda/D = 0.17$ of the dynamic lift force, η is calculated as 0.074 and 0.070, respectively, in the case of the large-scale model tests.

Fig. 9 shows the NPSD of the dynamic drag force measured in the large-scale model tests as a function of nondimensional frequency f^*. The NPSD Φ has almost the same characteristics as those of the small-scale model tests. In Fig. 9, the thick lines denote the correlation equations of Φ shown in Table 2. They show good quantitative agreement, though Φ of the large-scale model test is slightly larger than that of the small-scale model tests.

Fig. 10 shows the NPSD Φ of the dynamic lift force measured by the large-scale model tests and the correlation equation in the lift direction. They also agree with each other quantitatively, and no remarkable Reynolds effects are observed.

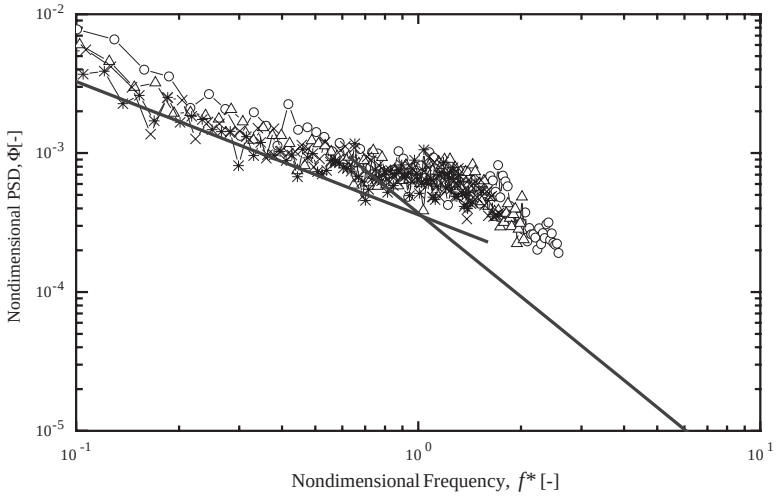

Fig. 9. NPSD of local dynamic drag force acting on the cross-shaped tube in the 3rd row. Reynolds number: —○—, 6.8×10^5; —△—, 8.4×10^5; —×—, 1.0×10^6; —✳—, 1.2×10^6. ——, correlation equation shown in Table 2.

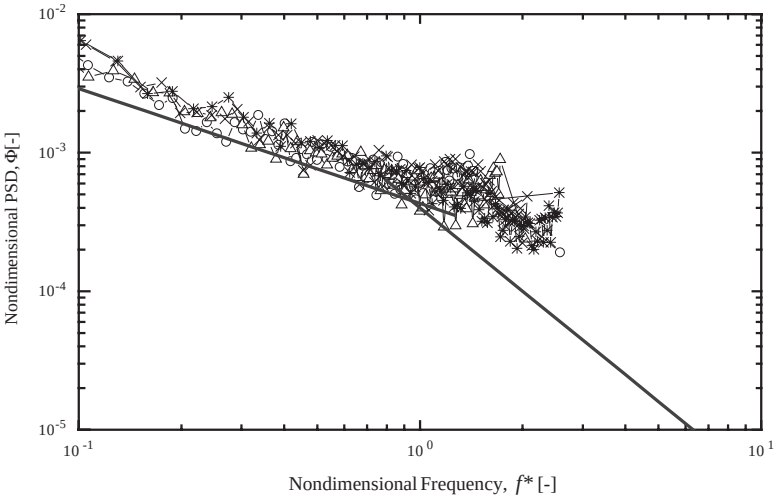

Fig. 10. NPSD of local dynamic lift force acting on the cross-shaped tube in the 3rd row. Reynolds number: —○—, 6.8×10^5; —△—, 8.4×10^5; —×—, 1.0×10^6; —✳—, 1.2×10^6. ——, correlation equation shown in Table 2.

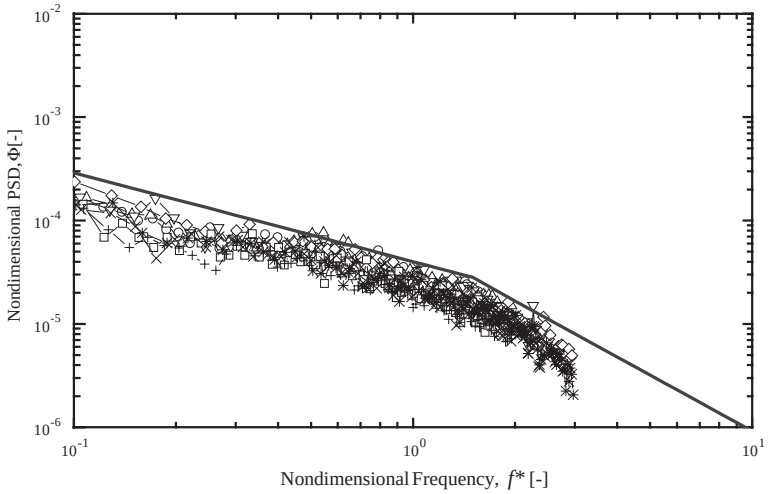

Fig. 11. NPSD of local dynamic torque acting on the cross-shaped tubes: —○—, 2nd row, $Re = 6.8 \times 10^5$; —△—, 2nd row, $Re = 8.4 \times 10^5$; —▽—, 2nd row, $Re = 1.0 \times 10^6$; —◇—, 2nd row, $Re = 1.2 \times 10^6$; —□—, 3rd row, $Re = 6.8 \times 10^5$; —+—, Re = 3rd row, 8.4×10^6; —×—, Re = 3rd row, 1.0×10^6; —✳—, 3rd row, 1.2×10^6. ——, envelope curve of NPSD.

Table 3
NPSD of local dynamic fluid torque acting on cross-shaped tube

Correlation length	0.16 (best fit)		
λ/D	0.40 (conservative)		
Correlation equation	Frequency condition	a_1	A_2
$\Phi(f^*) = a_1 f^{*a_2}$	$f^* < 1.5$	4.0×10^{-5}	−0.86
	$f^* > 1.5$	5.8×10^{-5}	−1.8

Hence, the above results suggest that the Reynolds number has little effect on dynamic drag and lift forces acting on cross-shaped tube bundles at least for $Re < 10^6$. However, Φ of the large-scale model tests is a little larger than that of the small-scale model tests, so a conservative correlation length is recommended for estimating the random vibration.

4.2. PSD of dynamic torque

The fluid dynamic torque acting on the cross-shaped tube bundle was also measured in the large-scale model tests. Given that the correlation length of the fluid dynamic torque is almost the same as for dynamic lift and drag, the fluid dynamic torque measured can be converted to the NPSD of the local fluid dynamic torque as follows:

$$\Phi(f^*) = \frac{S'(f)}{l^2 \psi_1(\eta) \left(\frac{1}{2}\rho U_g^2 D^2\right)^2 (D/U_g)}, \tag{18}$$

where $S'(f)$ is the PSD of the fluid dynamic torque measured in the large-scale model tests.

Fig. 11 shows the NPSD of the local dynamic torque in the large-scale model tests converted by using $\lambda/D = 0.16$. Again, the NPSD Φ of the local fluid dynamic torque has almost the same characteristics as for local dynamic lift and drag. Φ slowly decreases as nondimensional frequency increases, and falls a little more rapidly in the range of $f^* > 1 \sim 1.5$. Besides, no typical peaks of vortex shedding appear, and the NPSDs acting on the tube in the second row and the third row overlap one another. The envelope of the NPSD curves is also proposed as a correlation equation for the local dynamic torque in Table 3.

5. Examination of correlation equations of dynamic torque

As for random excitation force in the lift and drag directions, it is confirmed that the proposed correlation equations are reasonable and the Reynolds effects can be considered to be negligible by comparing the results of the small-scale model tests and the large-scale model tests. On the other hand, the fluid dynamic torque was measured only in the large-scale model tests and so the validity of the correlation equation and the Reynolds effect was not examined sufficiently. However, the sensing part of the small-scale model can detect either lift or drag in one test, and no torque can be detected because of the sensing mechanism.

Therefore, free oscillation tests with another small-scale model were conducted to measure the response amplitude of free oscillation by random excitation in the torsional direction. The results were then compared with the predicted amplitude by using the correlation equations shown in Table 3.

5.1. Experimental arrangement of free oscillation test

Fig. 12 schematically shows the small-scale model used for the free oscillation tests. The loop shown in Fig. 1 was used for the tests again, and the small-scale cross-shaped tubes were installed in a normal arrangement of four rows with four tubes per row. The reference diameter D is about 90 mm and the transverse pitch is about 75 mm and the minimum gap width is about 8 mm. Both ends of the 9 tubes in total were supported by slender aluminum rods of 4.5-mm diameter and 80-mm length. The torsional rigidity of the cross-shaped tube is sufficiently larger than that of the supporting rods so it can be regarded as a rigid shaft with both ends elastically supported by torsional springs. The torsional responses of the five numbered tubes were measured by the strain gauges attached to the supporting rod. The other seven tubes (colored gray in Fig. 13) were dummies rigidly fixed to the test-section. In the free oscillation tests, the range of the Reynolds number was $2.5\times10^4<\mathrm{Re}<4.2\times10^4$.

5.2. Comparison of the measured response and the predicted response

The torsional response of the cross-shaped tube having both ends elastically supported by a torsional spring can be estimated by the following methods.

It is assumed that the motion of a tube in the tube bundle is hardly coupled with those of adjacent tubes when the response amplitude of the tube is small. In this case, it is supposed that a tube elastically supported in the tube bundle can be considered to be a one-degree-of-freedom system. The motion equation of the rigid shaft elastically supported by a torsional spring is expressed as follows:

$$\ddot{\theta}+2\zeta_n\omega_n\dot{\theta}+\omega_n^2\theta=\frac{F_T(t)}{I_p}, \tag{19}$$

where θ is the angular displacement of the rigid shaft, $F_T(t)$ is random excitation torque, and I_p is the inertia moment including the added inertia moment of the shaft. The added inertia moment I_{aT} is calculated by

$$I_{aT}=K_T\frac{1}{128}\rho\pi D^4, \tag{20}$$

where $K_T=1.5$ (Inada et al., 2002).

With lightly damped structures, the root-mean-square amplitude of the response can be calculated as follows:

$$\sqrt{\overline{\theta^2}}=\sqrt{\sum\frac{S(f_n)}{64\pi^3I_p^2f_n^3\zeta_n}l^2\psi_1^2}, \tag{21}$$

where l is the spanwise length of the shaft, and S is the one-sided PSD of the local fluid dynamic torque. Using the correlation equations shown in Table 3, S is calculated as

$$S(f)=\left(\frac{1}{2}\rho U_g^2D^2\right)^2\Phi\left(\frac{fD}{U_g}\right)\frac{D}{U_g}. \tag{22}$$

Fig. 13 shows the root-mean-square amplitude of the torsional response measured by the free-oscillation tests and the amplitude predicted with the correlation equation, giving the damping ratio $\zeta_n=0.5\%$. They agree well quantitatively. Consequently, the proposed correlation equations appear to be appropriate, and the Reynolds effect can be considered negligible.

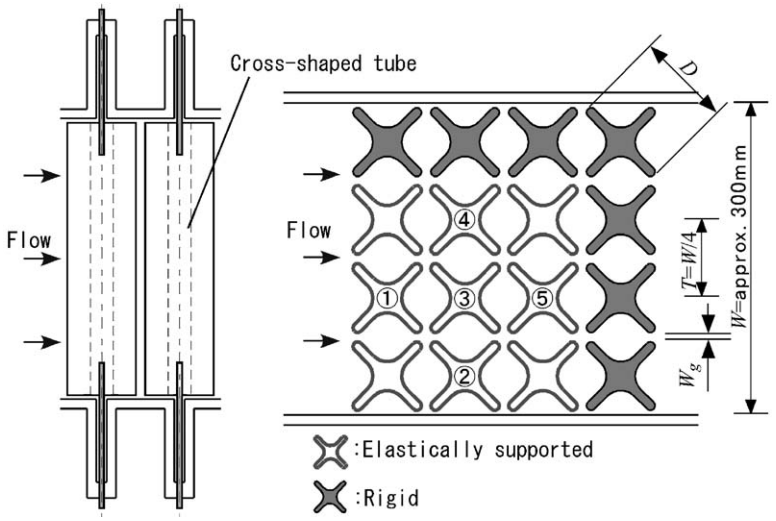

Fig. 12. Schematic of free oscillation test model of cross-shaped tube bundle.

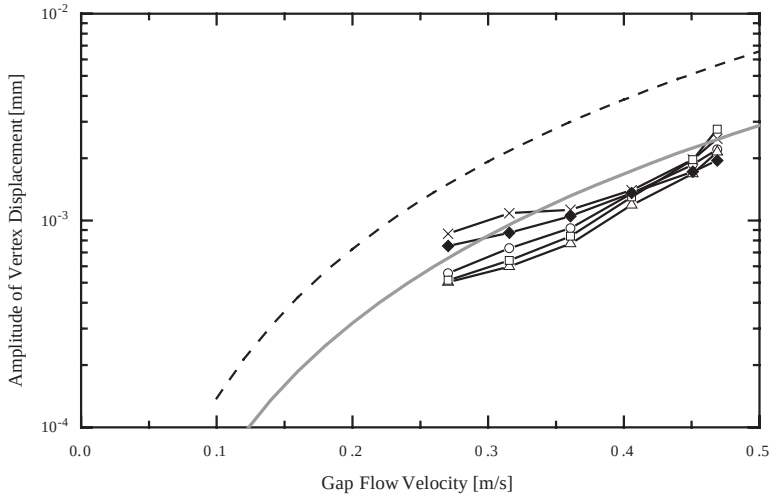

Fig. 13. Comparison of torsion response between experimental results and estimated value. r.m.s. amplitude: —○—, tube ①; —△—, tube ②; —×—, tube ③; —□—, tube ④; —◆—, tube ⑤; ——, the predicted (best estimate); ----, the predicted (conservative).

6. Conclusion

Fluid dynamic forces acting on a cross-shaped tube bundle in a normal arrangement subjected to cross-flow were measured by water tunnel tests with two types of scale model.

The results of the study can be summarized as follows.

(1) The measured fluid dynamic drag, lift and torque acting on the cross-shaped tube bundle in cross-flow were successfully compiled into correlation equations, which include the NPSD of the local fluid dynamic force and the spanwise correlation length. The results provide a universal spectrum and spanwise correlation length for evaluating the turbulence-induced vibration response of cross-shaped tube bundles in cross flow.

(2) The PSD of fluid dynamic drag, lift and torque acting on a cross-shaped tube bundle have mutually similar properties and they gradually decline as the frequency increases. No remarkable spectral peaks of vortex shedding appeared. The reason for this is considered to be that the ratio of gap width to tube diameter is small for the tested arrangement.

(3) The PSD of the fluid dynamic forces acting on the tube in the first row is smaller than those acting on the tubes downstream. The PSD is almost saturated downstream of the second row.
(4) The ratios of the correlation lengths to the tube diameter for the cross-shaped tube bundle are much shorter than that of the random excitation force acting on circular tube bundles. However, the ratio of the correlation length to the minimum gap width for the cross-shaped tube bundle agrees well with that for a circular tube bundle with a small pitch-to-diameter ratio. This implies that the correlation length might be proportional to the minimum gap width rather than the tube diameter when the ratio of the minimum gap width to tube diameter is very small.
(5) The Reynolds number effects on the nondimensional power spectral density of the local fluid dynamic force can be considered negligible at least in the range of Reynolds number $<10^6$.

References

ASME Boiler and Pressure Vessel Code, 1998. Sec. III Appendix N-1300, ASME.

Au-Yang, M.K., 1999. Joint and cross acceptances for cross flow-induced vibration; Part I: Theoretical and finite-element formulations. In: Flow-Induced Vibration, PVP Vol. 389. ASME, New York, pp. 17–24.

Au-Yang, M.K., 2001. Flow-Induced Vibration of Power and Process Plant Components, A Practical Workbook. ASME Press, New York.

Axisa, F., Antunes, F., Villard, B., 1990. Random excitation of heat exchanger tubes by cross-flows. Journal of Fluids and Structures 4, 321–341.

Blevins, R.D., 1990. Flow Induced Vibration, 2nd Edition. Van Nostrand Reinhold, New York.

Blevins, R.D., Gibert, R.J., Villard, B., 1981. Experiment on vibration of heat exchanger tube arrays in cross-flow. Transactions of the Sixth International Conference on Structural Mechanics in Reactor Technology, Paris, Paper B6/9.

Chen, S.S., 1987. Flow-Induced Vibration of Circular Cylindrical Structures. Hemisphere Publishing Corporation, Washington.

Chen, S.S., Jendrzejczyk, J.A., 1987. Fluid excitation forces acting on a square tube array. ASME Journal of Fluids Engineering 109, 415–423.

Inada, F., Yasuo, A., Kawamura, K., 1993. Statistical correlations of random fluid forces acting on a tube bundle in cross flow. Proceedings of Symposium on Flow-Induced Vibrations in Engineering Systems, Asia-Pacific Vibration Conference '93, Vol. 1, pp. 31–34.

Inada, F., Yoneda, K., Yasuo, A., Nishihara, T., 2001. A study on fluid excitation forces acting on a rotated square tube bundle of *T/D=3.1* in cross flow. Symposium on Flow-Induced Vibration, PVP 420-1. ASME, New York, pp. 87–94.

Inada, F., Nishihara, T., Yasuo, A., Morita, R., Sakashita, A., Mizutani, J., 2002. Self-excited vibration of cross-shaped tube bundle in cross flow. Fifth International Symposium on FSI, Aeroelasticity & FIV + Noise. ASME, New York.

Inada, F., Nishihara, T., Yasuo, A., Morita, R., Sakashita, A., Mizutani, J., 2003. Self-excited vibration of cross-shaped tube bundle in cross flow. Journal of Fluids and Structures 18, 651–661.

Pettigrew, M.J., Gorman, D.J., 1981. Vibration of heat exchanger tube bundles in liquid and two-phase cross flow. In: Chen, P.Y. (Ed.), Flow-Induced Vibration Design Guide-lines, PVP Vol. 52. ASME, New York, pp. 89–109.

Weaver, D.S., Fitzpatrick, J.A., 1988. A review of cross-flow induced vibrations in heat exchanger tube arrays. Journal of Fluids and Structures 2, 73–93.

Yamashita, N., et al., 2001. Evaluation of flow-induced vibration of cruciform control rod guide tubes using numerical flow analysis. SMIRT16, No. 2061, Washington, DC.